J Sol-Gel Sci Technol (2010) 53:148–153
DOI 10.1007/s10971-009-2070-7

ORIGINAL PAPER

Growth mechanism of Nb-doped TiO_2 sol–gel multilayer films characterized by SEM and focus/defocus TEM

Chun Wang · Jürgen Meinhardt · Peer Löbmann

Received: 23 April 2009 / Accepted: 26 August 2009 / Published online: 11 September 2009

Abstract TiO_2 and Nb-doped TiO_2 films were prepared by sol–gel processing, their microstructure was adjusted by varying the number of subsequent coating-firing cycles that resulted in final total film thickness of ~100 nm. When only few subsequent coatings are stacked (large single layer thickness) granular polycrystalline microstructures are observed. Doping with Nb reduces the crystallite size compared to the respective pure anatase films. When the single layer thickness is reduced, the film growth is successively dominated by the nucleation of subsequent films on the underlying crystalline material resulting in a columnar dense film structure. The multilayer architecture of such films can be demonstrated by defocus TEM imaging even if crystalline columns exceed single film boundaries. Results indicate that Nb is homogeneously incorporated into the anatase lattice by substitution of Ti, nevertheless the electric conductivity after H_2 post annealing is significantly lower than reported for analogous films prepared by magneton sputtering or pulsed laser deposition.

Keywords Thin films · TCO · Titanium dioxide · Nb-doping · TEM

1 Introduction

Sol–gel processing has evolved into a widely accepted technology for the preparation of inorganic and hybrid coatings from chemical precursors [1–3]. After drying of the solvent and complete removal of organic residues by thermal treatment crystalline films can be obtained ranging from "simple" materials such as TiO_2 [4] to complex compositions like lead-zirconate-titanate ($PbZr_xTi_{1-x}O_3$, PZT) [5] or yttrium-barium-copper oxide ($YBa_2Cu_3O_x$, YBCO) [6, 7]. The microstructure obtained is mostly fine-grained due to the crystallization of the amorphous film material as obtained after drying and pyrolysis of the residual organic moieties. The coatings additionally may retain some porosity and the tensile stresses which occur during the densification are known to cause cracking [8, 9]. Therefore, when dense films with large grains are required, vacuum-based technologies such as sputtering are often considered to be the better choice.

It has been demonstrated, though, that highly dense ceramic films can be obtained by sol–gel processing, too, when the material is deposited by multiple coating-firing cycles [10]. The columnar grain structure is explained by the nucleation of each film on the underlying material that has already been crystallized. When the single layer thickness is kept sufficiently low, this homoepitaxial growth overcompensates nucleation within the new film due to its large surface-to-volume ratio.

Schuler et al. [11, 12] described the microstructure of sol–gel films in terms of a "structural zone model" predicting microstructural features as a function of intrinsic grain size and single layer thickness. Multiple nucleation events (small grain sizes) in thick films (large single layer thickness) favor granular structures, whereas decreasing the single layer thickness leads to columnar structures as described above. Both growth regimes are separated by films that exhibit a "layered structure". These features may be explained by the stacking of single films that posses both "columnar regions" induced by the underlying solid and "granular regions" dominated by homogeneous

C. Wang · J. Meinhardt · P. Löbmann (✉)
Fraunhofer-Institut für Silicatforschung, Neunerplatz 2,
97082 Würzburg, Germany
e-mail: peer.loebmann@isc.fraunhofer.de; loebmann@isc.fhg.de

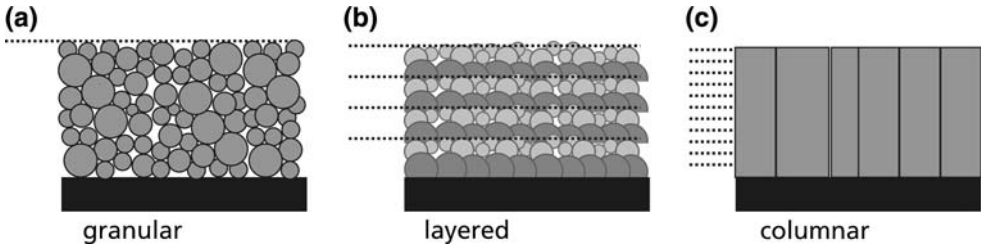

Fig. 1 Visualization of **a** granular, **b** layered and **c** columnar sol–gel film structures as classified by Schuler et al. [11]

nucleation within each newly deposited film. It recently has been shown that also the interface between sol–gel film and the atmosphere may induce the formation of an impermeable surface layer on top of a partially porous granular film [13]. The different film structures as classified by Schuler et al. are visualized in Fig. 1.

The performance of thin films of transparent conductive oxides (TCOs) critically depends on their microstructure. The conductivity of sol–gel derived indium-tin oxide [14] and aluminium-doped zinc oxide (AZO) films [15] are typically one order of magnitude lower than that of the respective materials prepared by vacuum-based technologies such as sputtering [16–18]. Nevertheless sol–gel processing is a very flexible method with respect to the variation of material composition and the introduction of dopants. Additionally 2-D microstructured films can be prepared by pad- or gravure-printing [19, 20].

Recently Nb-doped TiO_2 films showing high electric conductivities have been reported [21], samples with resistivities of 1.5 E-03 Ω cm and 9.5 E-04 have been prepared by pulsed laser deposition [22] and sputtering [23, 24], respectively. In this paper we describe the microstructure of TiO_2 and Nd-doped TiO_2 films prepared by multiple sol–gel dip-coating experiments.

2 Experimental procedure

TiO_2 precursor powders were prepared from titanium tetraethoxide using acetylacetone as chelating agent and water for hydrolysis reaction in a molar ratio of 1/1/3. After hydrolysis all volatile components were removed by rotational evaporation to yield a soluble precursor powder. Coating solutions were prepared by the dissolution of the precursor powders in mixtures containing 90 mass% ethanol and 10 mass% 1,5-pentanediol. More detailed information about the precursor powder synthesis and the preparation of coating solutions was previously reported [4, 9, 25].

Nb-doped TiO_2 sols were prepared by addition of $Nb(OEt)_5$ to the solutions, a molar ratio Ti/Nb of 94:6 was chosen. The concentration of the coating solutions was adjusted to an oxide yield of 6 mass% with respect to TiO_2 and $Ti_{.94}Nb_{.06}O_{2-x}$.

The withdrawal rates of dip coating experiments were varied to adjust different single layer thickness', the respective coating-firing cycles were repeated until a final multilayer thickness of 100 ± 15 nm was obtained. The samples were treated in a furnace pre-heated to 600° for 10 min after each coating.

Film thickness was calculated from UV–VIS reflection spectra of the samples (UV–Vis spectrometer, Shimadzu UV-3100, Kyoto, Japan) using the Swanepoel method [26].

The film resistivities were measured by a Keithley 199 System DMM Scanner by a two point measurement. A fixed area of the film was masked with an adhesive tape and silver varnish was painted onto the opposing outer rims, whereupon the electrodes were placed after drying. Due to the high resistivity of the films, the usual van-der-Pauw four point methods could not be applied.

The films with their glass substrates were cut into about 1 cm^2 pieces and fixed on the SEM sample holders in edged-on and faced-on manners, respectively. Prior to investigation, the edged-on samples were sputter-coated with Pt to avoid charging. The images were acquired with an in-lens detector at the working distance of 3 mm, by using the accelerating voltage of 2 kV (Field Emmision SEM, Ultra 55, Carl Zeiss NTS Inc. Oberkochen, Germany). The samples for TEM investigation were prepared with focused ion beam instrument (Dual Beam FIB/SEM, Quanta 200 3D, FEI Company, Eindhoven, The Netherlands). The surface of the films were covered with 20 nm dense Pt-sputtered layers, the rest sides of the glass slices were coated with conductive silver. In this way, the sample was completely enveloped in conductive shells so that the charging and drifting during FIB cutting can be reduced into tolerant extends.

The TEM investigation was performed with Jeol 2010 (Jeol Ltd, Tokyo, Japan: LaB6 filament, at accelerating voltage of 200 kV, point resolution of 0.24 nm, plane resolution of 0.14 nm, spherical aberration coefficient Cs = 1.0 mm, chromic aberration coefficient Cc = 1.4 mm. The images were captured and analysed with DigitalMicrograph (camera type 794 MSC) (Gatan Inc. Pleasanton, CA 94588, USA). EDX experiments were carried out with the EDAX instrument attached on the TEM column analysed with Genesis Spectrum software (EDAX Inc., Mahwah, NJ, USA).

The crystallographic phases and the lattice parameters of the pure TiO_2 and Nb doped TiO_2 films (30-fold coatings, respectively) were determined with X-ray diffractometer (Siemens D5005, Karlsruhe. Germany) with CuKα radiation ($\lambda = 1.5408$ Å).

3 Results and discussion

Irrespective of the number of subsequent single layers applied to obtain the final thickness of 100 ± 15 nm, the TiO_2 and Nb-doped TiO_2 films could be prepared without any microscopic cracks or any visual defects.

Anatase was the only phase detected by XRD, no traces of rutile or Nb_2O_3 were found (Fig. 2). In Fig. 3 the crystallite sizes as determined by the Scherer-equation are compared. When the final film is composed of 5–30 layers (single layer thickness below 20 nm) the results for doped and undoped films do not significantly differ: The crystallite size increases from approx. 18 nm for a single layer thickness of 20 nm to approx. 38 nm for single layer thickness of 4 nm. A grain size exceeding the single layer thickness fully agrees with the assumption of an epitaxial "columnar" film growth as classified by Schuler et al. [11, 12].

For higher single layer thickness' smaller crystallite sizes are observed for Nb-doped TiO_2 than for pure titania. A granular-polycrystalline microstructure is predicted as a consequence of homogeneous nucleation events in the larger volumes of thicker single layers [11]. The difference

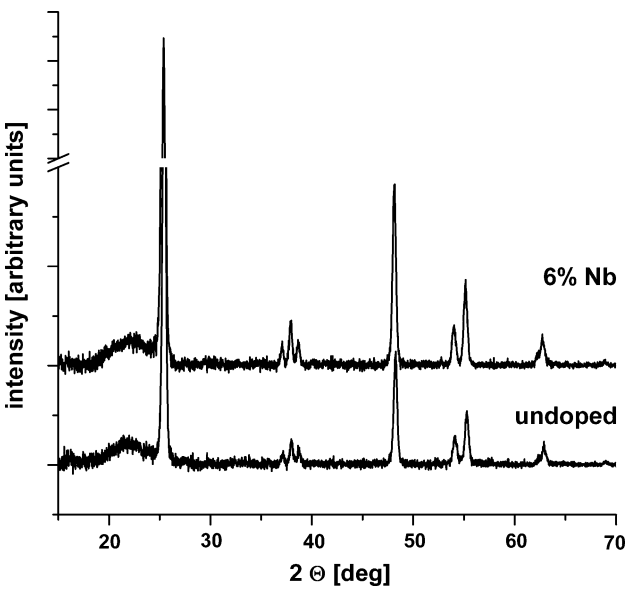

Fig. 2 XRD-pattern of undoped TiO_2 thin film (*bottom*) and film doped with 6% Nb (*top*). The films with final thickness' of 100 ± 15 nm were deposited by 30-fold coating-firing cycles, respectively

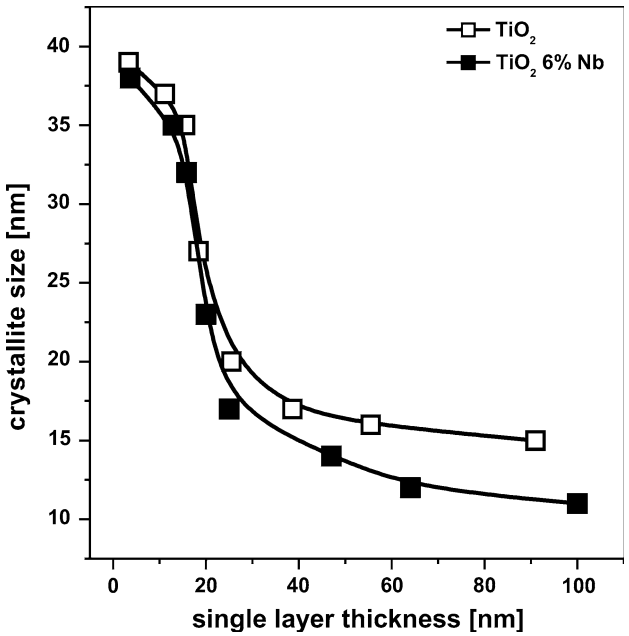

Fig. 3 Crystallite size of TiO_2 (*open square*) and Nb-doped TiO_2 (*filled square*) films determined by XRD-measurements as function of single layer thickness. The final multilayer assemblies had an overall thickness of 100 ± 15 nm

observed in Fig. 3 suggest that the presence of Nb increases the number of homogenous nucleation sites for the crystallization of TiO_2 resulting in a finer grained polycrystalline structure. Alternatively if it is assumed that the presence of the dopant retards the growth rate of the crystallites during thermal treatment as e.g. observed for Fe-doped TiO_2 [27], a larger number of seeds may have time to emerge which also explains the smaller grain size.

The microstructure of different films was characterized by electron microscopy. As no significant differences between pure TiO_2 films and doped material was observed in the resolution provided by SEM, only images corresponding to TiO_2 containing 6% Niobium are shown. In Fig. 4 surface images of 3-, 5-, 6- and 30-fold coatings are given, the respective cross-sectional views are summarized in Fig. 5.

The surface of the film prepared by three subsequent coating-firing cycles (Fig. 4a) shows spherical grains. Their average size (20 ± 3 nm) corresponds to the crystallite size determined by XRD in the range of the error of image analysis. Larger structures are visible in the respective cross sectional SEM image (Fig. 5a) suggesting that they consist of aggregates of several smaller grains. It recently has been shown that partially porous sol–gel films can be separated from the environment by a dense surface layer [13] which presumably is generated by heterogeneous nucleation at the film-atmosphere interface during thermal treatment. This accounts for the observed difference between surface and cross sectional images.

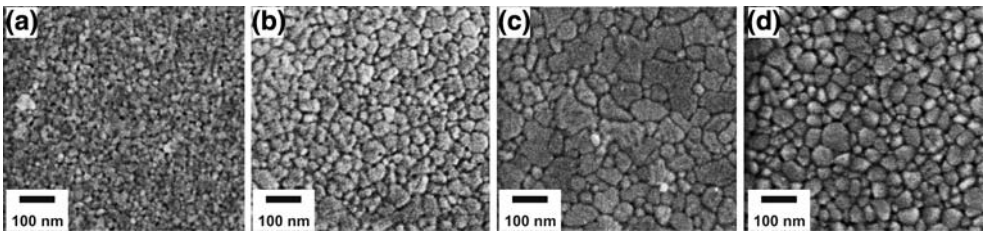

Fig. 4 Surface SEM images of Nb-doped TiO_2 films prepared by 3-fold (**a**), 5-fold (**b**), 6-fold (**c**) and 30-fold (**d**) subsequent coating-firing cycles. The single layer thickness' were determined as 37, 21, 16 and 3.7 nm, respectively

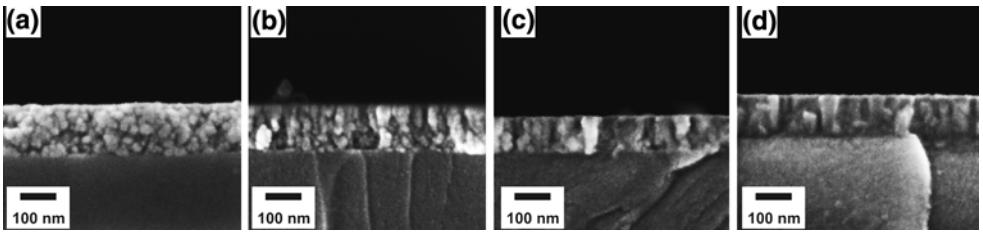

Fig. 5 Cross-sectional view by SEM at fractured surfaces of the samples from Fig. 4

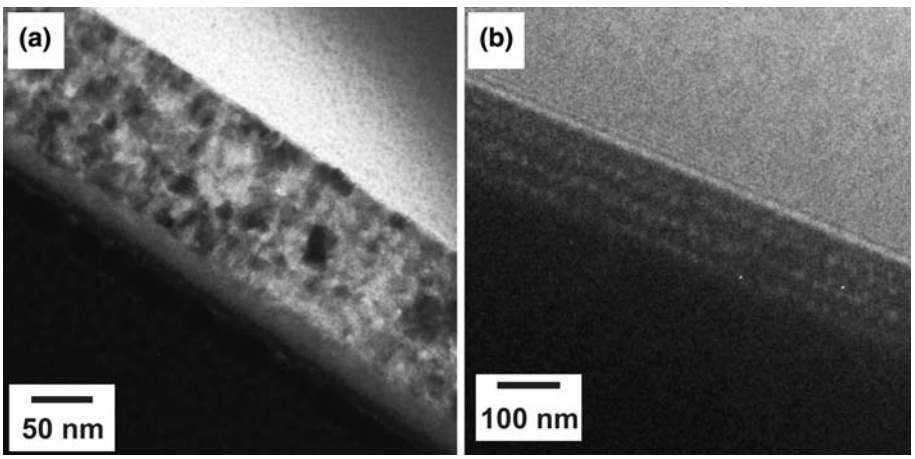

Fig. 6 Cross-sectional views of three-fold Nb-doped TiO_2 coatings by TEM. The focused image is given in, (**a**) the single layers can be distinguished in the defocus Fresnel image (**b**) only

The fivefold coating also generates a granular film, its surface structure is coarser (33 ± 17 nm) than for samples prepared by threefold coating (Fig. 4b). The cross-sectional view of the films (Fig. 5b) suggests the presence of elongated grains on top of a rather spherical-granular film structure near the substrate.

If the film is prepared by six subsequent coating-firing cycles, a columnar film structure becomes apparent in the cross sectional view (Fig. 5c), single grains range from the substrate up to the film surface. The grain size observed by surface imaging also increases to 48 ± 30 nm (Fig. 4c), the large standard deviation indicates the coexistence of small and larger grains. These structural changes observed for five- and six-fold coatings coincides with the significant increase of crystallite size as determined by XRD (Fig. 2) for the films with a single layer thickness below 20 nm.

Films built up by 30 single layers also consist of columnar grains (Fig. 5d). The surface image analysis (Fig. 4d) yields grain sizes of 34 ± 16 nm. This value is slightly below the crystallite size derived from the diffraction data, because the top-view on a columnar grain does not represent its maximum/average dimension. Since no deviation of the XRD intensity ratios (Fig. 2) is observed in comparison to the reference pattern, the columns do not have a preferred crystallographic orientation. The standard deviation of the grain size derived from surface image analysis is significantly lower than that of five- and six-fold coatings. This observation indicates that further film growth by adding thin single layers proceeds by the growth of larger grains at the expense of small crystallites; a more stable growth regime is established than for higher single layer thicknesses.

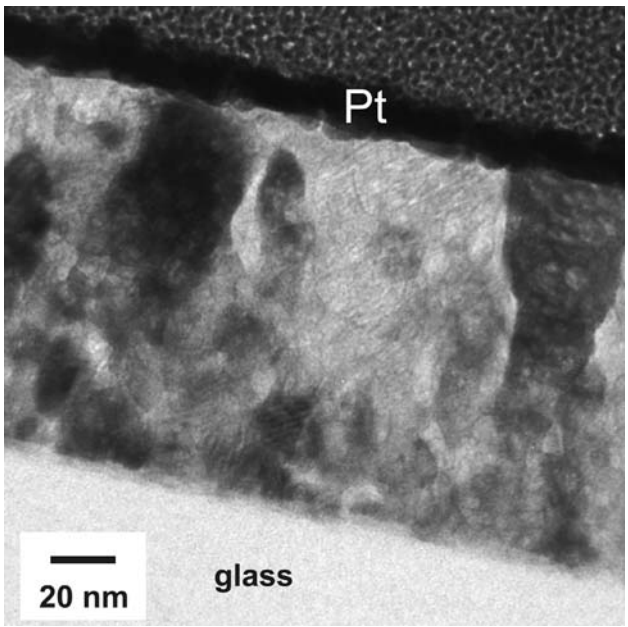

Fig. 7 Cross-sectional view of five-fold Nb-doped TiO_2 coatings by TEM. The image shows the transition of a granular film structure in regions near the substrate to columnar growth regime

In contrast to reports on sol–gel prepared AZO films [12], no intermediate "layered structure" is observed by SEM. The TEM micrographs in Fig. 6 display a triple coating corresponding to Figs. 4a and 5a. The focused image of Fig. 6a clearly shows a homogeneous granular film structure, whereas the three subsequent layers can be distinguished in the defocused Fresnel image of Fig. 6b.

This difference between the images can be rationalized by the particle-wave dualism of electrons: at in-focus setting the amplitude of the electron wave is zero at the specimen level, the image contrast relies only on the particle property.

If the electron beam is at defocus setting the phase and the amplitude of the electron wave can be changed differently: when the front of electrons passing through media with (slight) differences in inner potential, phase and the amplitude of the electron wave can be changed differently which results in image contrast. The layers apparent in the defocus image of Fig. 6b thus correlate to marginal gradients in film density, that are not perceptible in Fig. 6a.

In Fig. 7 the microstructural feature found in a cross sectional TEM view of a fivefold coating is given. For this sample the SEM image (Fig. 5b) had suggested a columnar structure near the surface on top of a more granular region adjacent to the substrate. In contrast to some other areas of the specimen, where TiO_2 crystallites already range from the substrate to the film surface (completely columnar film structure), columnar grains emerge from a polycrystalline region adjacent to the glass substrate. At this spot the second or third coating did not nucleate sufficiently on the underlying TiO_2, a satisfactory epitaxial growth is only established for the upper layers. This instructive "snapshot" visualizes growth regimes dominated by multiple (polycrystalline) nucleation and by homoepitaxial growth within one film.

The TEM image in Fig. 8 reveals the dense and highly ordered columnar microstructure of a 30-fold coating (single layer thickness 3.4 nm). Even though the columnar grains ranging from substrate to film surface are single crystals, the single layers still may be identified in the defocused Fresnel image of Fig. 8b. These features do not correspond to lattice fringes.

The presence of Nb was verified by TEM-EDX for doped samples, neither the accumulation of Nb close to grain boundaries nor a concentration gradient throughout columnar films could be determined. The dimension of the unit cell (tetragonal, $a = b = 0.37908$ nm, $c = 0.95298$ nm) as determined by analysis of the X-ray diffraction pattern is slightly enlarged compared to pure anatase (tetragonal, $a = b = 0.37852$ nm, $c = 0.95139$ nm) as one would

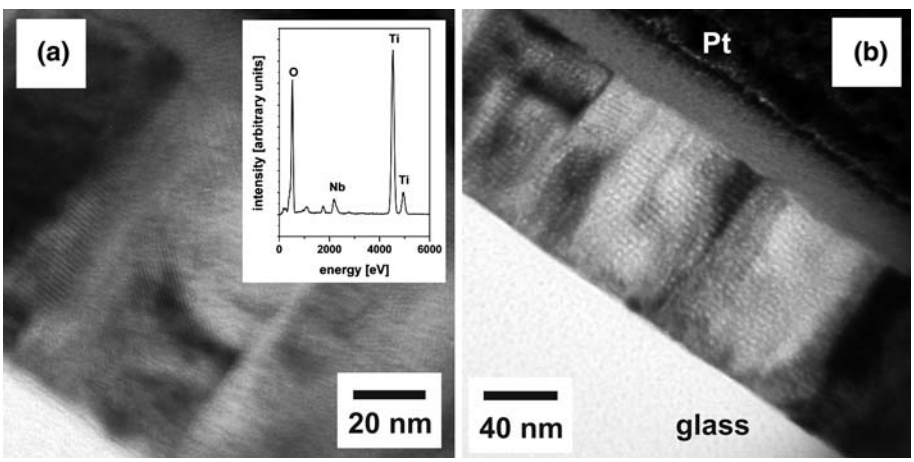

Fig. 8 Cross-sectional views of 30-fold Nb-doped TiO_2 coatings by TEM. The focused image, (**a**) shows ordered columnar grains extending from the substrate to the film surface, whereas in the defocus Fresnel image (**b**) vertical features corresponding to the single coatings still can be distinguished. The *inset* in (**a**) displays an EDX spectrum of the respective sample

expect in the case of homogeneous distribution of the dopant in the lattice [21].

Nb-doped TiO_2 films were post annealed at 600 °C in pure hydrogen. The resistivity of these samples (minimum 1.8 Ω cm), though, is 3 orders of magnitude higher than that of films with similar chemical composition prepared by PLD and sputtering [22–24]. Even though the thickness of those films is comparable to our sol–gel derived samples, their lateral crystallite size of several micrometers is considerably higher [23]. As the columnar grains of sol–gel Nb-doped TiO_2 films have diameters below 100 nm, higher grain-boundary scattering may reduce electron mobility and thus account for their inferior electric performance.

4 Conclusions

Granular and columnar films were obtained as predicted by the structural zone model. For intermediate single layer thicknesses no layered structures as reported in the literature but the switch from a granular to columnar growth regime was observed within one stacked multilayer. Additionally vertical features corresponding to the single coatings still can be distinguished by defocus Fresnel TEM imaging in the crystalline columns that range from the substrate to the film surface.

Nb-doped TiO_2 films with a composition similar to that reported using pulsed laser deposition were obtained, nevertheless their resistivity is three orders of magnitude lower even though the investigations indicate a homogeneous distribution of Nb in the TiO_2 lattice. Further studies aim at the explanation of the different performance and the optimization of the sol–gel derived films.

Acknowledgments This work has been funded within the framework METCO of the Fraunhofer-Gesellschaft. The authors gratefully acknowledge Annett Halbhuber's careful and accurate dedication to the preparation of multiple coatings.

References

1. Brinker C, Scherer G (1990) Sol–gel science—the physics and chemistry of sol–gel processing. Academic Press, Boston
2. Schottner G (2001) Chem Mater 13:3422
3. Mackenzie J (2003) J Sol–Gel Sci Technol 26:23
4. Bockmeyer M, Löbmann P (2006) Chem Mater 18:4478
5. Reaney I, Taylor D, Brooks K (1998) J Sol–Gel Sci Technol 13:813
6. Risse G, Schlobach B, Haessler W, Stephan D, Fahr T, Fischer F (1999) J Eur Ceram Soc 19:125
7. Wang S, Qiu L, Wang L, Du P, Chen S, Han Z (2005) Supercond Sci Technol 18:1271
8. Kozuka H, Takenaka S, Tokita H, Hirano T, Higashi Y, Hamatani T (2003) J Sol–Gel Sci Technol 26:681
9. Bockmeyer M, Löbmann P (2007) Thin Solid Films 515:5212
10. Schuler T, Aegerter M (1999) Thin Solid Films 351:125
11. Schuler T, Krajewski T, Grobelsek I, Aergerter M (2004) J Sol–Gel Sci Techno 31:235
12. Schuler T, Krajewski T, Grobelsek I, Aergerter M (2006) Thin Solid Films 502:67
13. Bockmeyer M, Herbig B, Löbmann P (2009) Thin Solid Films 517:1596
14. Beaurain A, Luxembourg D, Dufour C, Koncar V, Capoen B, Bouazaoui M (2008) Thin Solid Films 516:4102
15. Lin K, Tsai P (2007) Thin Solid Films 515:8601
16. Szyszka B (2001) Vakuum Forsch Prax 1:38
17. Minami T (2005) Semicond Sci Technol 20:S35
18. Schmidt-Mende L, MacManus-Driscoll J (2007) MaterialsToday 10(5):40
19. Puetz M, Aegerter M (2008) Thin Solid Films 516:4495
20. Prodi-Schwab A, Luethge T, Jahn R, Herbig B, Loebmann P (2008) J Sol–Gel Sci Technol 47:68
21. Furubayashi Y, Hitosugi T, Yamamoto Y, Hirose Y, Kinoda G, Inaba K, Shimada T, Hasegawa T (2006) Thin Solid Films 496:157
22. Hitosugi T, Ueda A, Furubayashi Y, Hirose Y, Konuma S, Shimada T, Hasegawa T (2007) Jpn J Appl Phys 46(3):L86
23. Yamada N, Hitosugi T, Hoang N, Furubayashi Y, Hirose Y, Shimada T, Hasegawa T (2007) Jpn J Appl Phys 46(8A):5275
24. Sato Y, Akizuki H, Kamiyama T, Shigesato Y (2008) Thin Solid Films 516:5758
25. Löbmann P (2005) J Sol–Gel Sci Technol 33:275
26. Diaz-Parralejo A, Caruso R, Ortiz A, Guiberteau F (2004) Thin Solid Films 458:92
27. Zhang Y, Reller A (2002) Mater Sci Eng C 19:323